

# Soft Tissue Prediction in Computer Assisted Maxillofacial Surgery Planning

## A Quantitative Evaluation of Histomechanical Modeling using Pre- and Postoperative CT-Data

S. Zachow, M. Weiser, H.-C. Hege, and P. Deußhard

Zuse-Institute Berlin (ZIB), Germany  
<[zachow,weiser,hege,deuffhard](mailto:zachow,weiser,hege,deuffhard@zib.de)>@zib.de  
[www.zib.de/visual/projects/cas](http://www.zib.de/visual/projects/cas)

**Abstract.** The aim of our work is to provide maxillofacial surgeons with a computer assisted 3D planning environment for complex bone relocations, facilitating a preoperative assessment of functional as well as esthetic rehabilitation. On this account we are developing an interactive simulation and visualization system and try to establish a robust modeling framework based on a biomechanical soft tissue model that can be used for a reliable prediction of a postoperative facial appearance. For that purpose homogeneous as well as inhomogeneous tissue models are investigated. Tissue deformations are computed with a finite element approximation on a tetrahedral discretization of the patients' facial soft tissue. For more than 30 patients a preoperative planning has been performed, and for 4 patients with distinct mid-facial hypoplasia the simulation results of maxillary advancements are quantitatively compared to the actual results, that are documented with postoperative tomographic data. This comparison enables us to assess the prediction quality of our simulation approach as well as to inversely determine suitable histomechanical parameters. In conclusion, a survey of advanced modeling aspects is presented, that we believe will improve facial tissue prediction.

## 1 INTRODUCTION

In maxillofacial surgery, physicians are often faced with skeletal malformations that require complex bone relocations. Especially in severe cases of congenital dysgnathia (misalignment of upper and lower jaw) or hemifacial microsomia (asymmetric bone and tissue development), where multiple bone segments are to be mobilized and relocated simultaneously and in relation to each other, careful preoperative planning is mandatory. At present in clinical routine the esthetic outcome, i.e. the postoperative facial appearance, can only be estimated by a surgeon's experience and hardly communicated to the patient. On this account, a preoperative planning of different therapeutic strategies, under consideration of functional rehabilitation and soft tissue deformation, is highly desired by maxillofacial surgeons [1]. The determination, verification, and optimization of adequate histomechanical soft tissue models for surgery planning and simulation is subject of current research [2, 3]. At Zuse-Institute in Berlin (ZIB) a computer assisted 3D surgery planning environment is being developed, that enables a surgeon to perform bone cuts and bone rearrangements in an intuitive manner on *virtual* patient models, including a prediction of the patients' postoperative appearance [4]. In collaboration with different surgeons and hospitals, we have demonstrated with more than 30 cases that our modeling and simulation approach is sustainable and provides a valuable planning criterion for maxillofacial surgeons as well as a demonstrative information for patients and their relatives.

## 2 SURGERY PLANNING WITH SOFT TISSUE PREDICTION

Before we are going to present a quantitative evaluation of simulation results we will give a short overview of our surgery planning environment, that is being developed at ZIB on basis of our 3D modeling and visualization system AMIRA [5]. In contrast to related works [6–9] we concentrate on the following three major problems to provide an integrated planning environment for cranio-maxillofacial surgery: (i) reconstruction of adequate 3D patient models from tomographic data, (ii) intuitive surgery planning of bone cuts (osteotomies) and bone relocations, and (iii) fast and robust simulation of the resulting facial appearance [10].

### 2.1 3D Patient Models

For a meaningful planning of surgical procedures, anatomically correct patient models providing all relevant details are required. Such models, being reconstructed from stacks of tomographic slices using AMIRA's segmentation tools, must contain at least the surfaces of bony structures with sufficient detail for osteotomy planning, as well as *all* surfaces completely bounding the volume of soft tissue (Fig. 1). The inner and outer tissue boundaries are needed for the generation of volumetric grids that represent a discretized computational domain for the numerical solution of the partial differential equations, describing tissue deformation in 3D elastomechanics [11].

All surfaces are initially reconstructed with subvoxel accuracy [12, 13], thus consisting of several million triangles, depending on the inner-slice resolution and the inter-slice distance (Fig. 1).

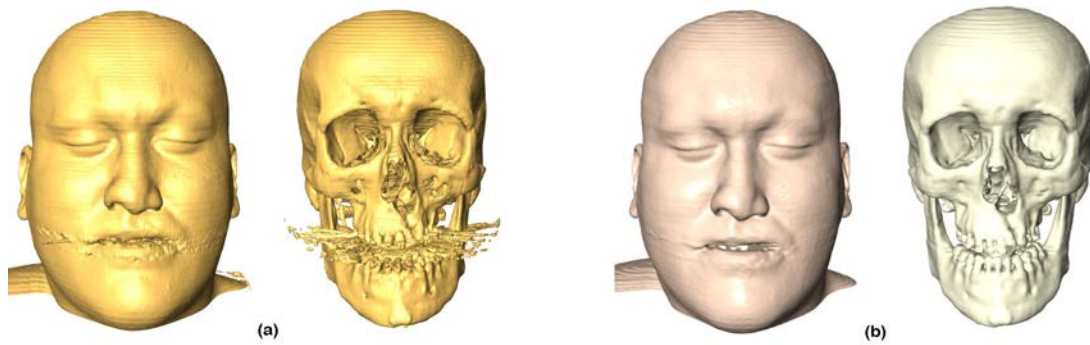


**Fig. 1.** a) Iso-surfaces of skin and bone with motion and metal artifacts, b) high resolution model consisting of 3.5 million triangles after segmentation

Since high resolution surface models are very demanding in view of interactive visualization and manipulation, and also lead to very high resolution volumetric grids, being far too large for fast finite-element simulations, a mesh simplification based on error quadrics is applied. To locally control the resolution, the original algorithm [14] has been extended to consider maximum edge length information per triangle as additional cost values for successive edge collapse. These values can be specified for different surface areas or automatically computed from the tissue thickness with the goal of providing a good basis for the generation of volumetric grids. Unstructured tetrahedral grids are then generated from these closed triangulations using a modified *Advancing Front* algorithm [15, 16]. Since a major requirement for fast finite-element analysis is a coarse mesh with optimally shaped elements, the placement of inner nodes is controlled with a 3D scalar field of edge length information, that can be computed from the edge lengths of the planning model up to a given maximum element size. Thus, starting from surface models consisting of 3 to 5 million triangles, planning models with a resolution of 75 000 to 150 000 triangles are constructed (Fig. 2 a). The simplification error, measured as deviation between initial and reduced surface model, always lies within a submillimeter range (0.1 - 0.5 mm). The resulting tissue grids typically consist of 175 000 to 500 000 tetrahedra (Fig. 2 c).

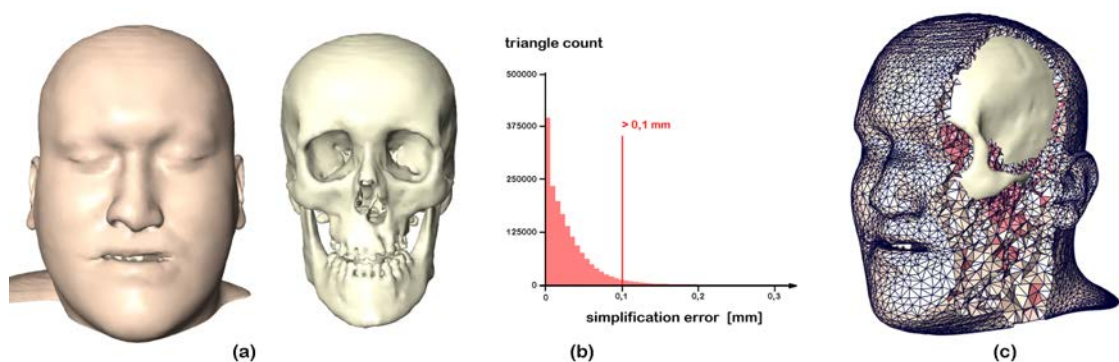


**Fig. 2.** a) Simplified 3D planning model (175 000 triangles), b) histogram of the simplification error per triangle, c) soft tissue grid with embedded skull (300 000 tetrahedra)

## 2.2 Osteotomy Planning and Bone Relocation

The planning of osteotomies (bone cuts) for the mobilization and relocation of bone segments is performed in accordance to the planning on basis of life size replicas of a patient's skull, i.e. stereolithographic models as shown in Figure 3 a. Osteotomy lines are drawn on top of the polygonal planning models (Fig. 3 b). After evaluation of the consequence of a planned cut with regard to vulnerable inner structures (nerves, teeth etc., Fig. 3 c), the model is separated accordingly [17]. A relocation of bone segments can be performed unrestricted in 3D or restricted to a translation or rotation within arbitrarily chosen planes. Bone and tooth collisions can be evaluated for functional analysis or orthodontic treatment planning. As a result of the preoperative planning, a single transformation matrix, encoding translation and rotation, or a sequence of such matrices will be provided for each bone segment. Both the osteotomy paths and the transformation parameters can finally be used for intraoperative navigation [18].

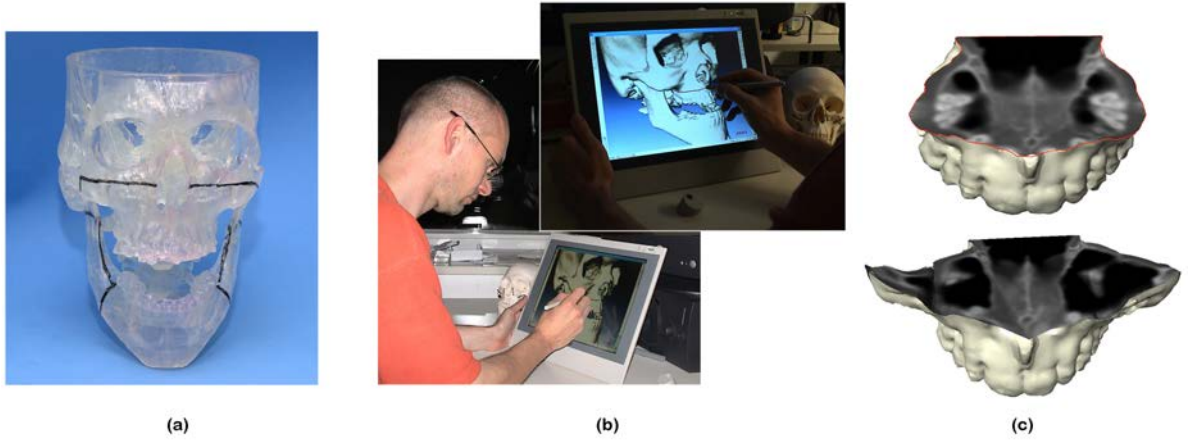


**Fig. 3.** Osteotomy planning: a) on a stereolithographic model, b) on a polygonal skull model, c) assessment of variants of a high Le Fort-I osteotomy with regard to vulnerable inner structures

## 2.3 Prediction of the Postoperative Facial Appearance

The relocated positions of bone segments serve as input for the simulation of soft tissue deformation. Since bone and surrounding soft tissue share boundaries that are either fixed or transformed, the resulting tissue configuration can be computed from the given boundary displacements  $\mathbf{u}|_{\Gamma_D}$ , in conjunction with properly assigned boundary types, by minimizing the deformation energy  $W$ .

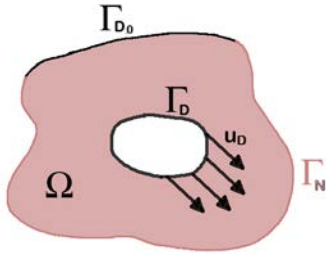
$$W := \int_V \frac{1}{2} \boldsymbol{\varepsilon} : \boldsymbol{\sigma} dV - \int_V \mathbf{f}_{ext} \cdot \mathbf{u} dV - \int_A (\boldsymbol{\sigma} \cdot \mathbf{n}) \cdot \mathbf{u} dA \quad (1)$$

In (1), the first integral term describes the internal energy, being induced by strains and resulting stresses, represented by the two tensors  $\boldsymbol{\varepsilon}$  and  $\boldsymbol{\sigma}$  respectively. The second term comprises external volume forces, like gravity, acting on the body, and the third contains normal stresses acting on the free part of the body's surface. In a stable static equilibrium, internal and external

forces are in balance, and deformation energy attains a local minimum. Since we only prescribe boundary displacements and neglect gravity, the latter two integrals in (1) vanish. Thus, tissue prediction can be reduced to numerically finding the minimum of the first integral (2) as a function of the displacements  $\mathbf{u}$  within the computational domain  $\Omega$  (cf. Fig. 4), e.g. using a finite element method.

$$W(\mathbf{u}) := \frac{1}{2} \int_{\Omega} \boldsymbol{\varepsilon} : \boldsymbol{\sigma} dV \longrightarrow \min \quad (2)$$

Stresses  $\boldsymbol{\sigma}$  are related to strains  $\boldsymbol{\varepsilon}$  via a constitutive law. In a first investigation, soft tissue is modeled as an isotropic and linear elastic ST. VENANT-KIRCHHOFF material, characterized by two independent elastic constants, POISSON's ratio  $\nu$  and YOUNG's modulus  $E$ . Strains are described by the linearized CAUCHY strain tensor  $\boldsymbol{\varepsilon}(\mathbf{u}) = \frac{1}{2}(\nabla \mathbf{u} + (\nabla \mathbf{u})^T)$  [4]. Based on these assumptions, the following system of partial differential equations (3), the so called LAMÉ-NAVIER equation [19], is solved for the given boundary conditions (4) using our finite-element software KASKADE [20].



$$\frac{E}{2(1+\nu)} \left( \frac{1}{1-2\nu} \nabla(\nabla \cdot \mathbf{u}(\mathbf{x})) + \Delta \mathbf{u}(\mathbf{x}) \right) = 0 \quad \text{in } \Omega \quad (3)$$

$$\mathbf{u}(\mathbf{x}) = \mathbf{u}_{D_0}(\mathbf{x}), \quad \mathbf{x} \in \Gamma_{D_0} \subset \partial\Omega$$

$$\mathbf{u}(\mathbf{x}) = \mathbf{u}_D(\mathbf{x}), \quad \mathbf{x} \in \Gamma_D \subset \partial\Omega \quad (4)$$

$$\boldsymbol{\sigma}(\mathbf{x}) \cdot \mathbf{n} = 0, \quad \mathbf{x} \in \Gamma_N \subset \partial\Omega$$

**Fig. 4.** Boundary conditions

### 3 QUANTITATIVE EVALUATION OF SIMULATION RESULTS

More than 30 treatments have been accompanied by preoperative planning so far. However, a validation of the prediction results on basis of postoperative photographs, as happened in most of the cases, is not sufficient. Although a validation with analytical solutions and simpler geometries, e.g. from the so called *truth cube* study [21], have proven that a 3D deformation can be computed correctly, the aim was to quantitatively validate the 3D soft tissue prediction with postoperative results. The department of oral and maxillofacial surgery of the University Hospital Leipzig in Germany evaluates a retention plate technique for midfacial distraction osteogenesis [22]. For the studies of bone development postsurgical CT data are acquired [23]. Four patients with distinct midfacial hypoplasia and class III dysgnathia, as shown in Figure 5, received presurgical treatment planning including soft tissue prediction for such a treatment. The simulation results can thus be verified on the basis of postoperative CT data.



**Fig. 5.** Patients with midfacial hypoplasia and ANGLE class III dysgnathia

The complete therapy planning, including osteotomy selection, bone cutting, maxillary advancement, and assessment of the dental occlusion as well as a 3D soft tissue prediction was performed with our surgery planning and simulation environment as explained in Section 2. In three cases, approximately two weeks after removal of the retention system a second CT was acquired for postoperative follow-up (Fig. 6). In a fourth case, the second CT was taken 8 weeks later in order to reduce swelling effects. For all pre- and postoperative scans the same imaging systems, either a Siemens Somatom Plus 4 or a Siemens Volume Zoom were used with equally chosen scan parameters and special attention to a minimum dose distribution [24]. Solely the fields of view and the head positions were differing slightly.

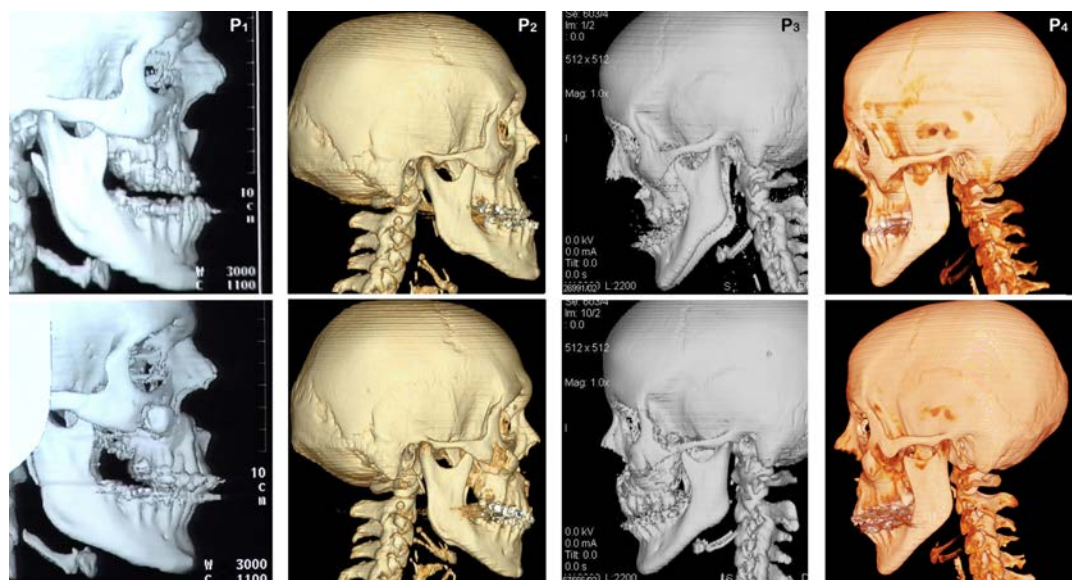


**Fig. 6.** CT data sets of the patients in Fig. 5: top) preoperative, bottom) postoperative

In order to be able to compare the simulated soft tissue deformation with the true postoperative outcome, the performed surgery was to be reproduced accurately with regard to the exact bone relocation. Only an accurate reproduction of the postsurgical result enables us to quantitatively assess our simulation results, and to inversely determine suitable histomechanic parameters for improving our modeling approach [25].

### 3.1 Corresponding Pre- and Postoperative 3D Models

To get a comparable reconstruction of bone with regard to its volume, a suitable segmentation threshold has been identified within each pair of corresponding data sets. These values were determined by comparison of the bone volume (e.g. the hyoid) in the pre- and the postoperative CT data. In one case, for instance, a threshold of 195 HOUNSFIELD units (HU) was chosen for the preoperative data set with a voxel size of  $0.41 \times 0.41 \times 1 \text{ mm}^3$ , resulting in a volume of  $1.471 \text{ cm}^3$ . For the postoperative data a threshold of 180 HU lead to an equivalent volume of  $1.473 \text{ cm}^3$  with a voxel size of  $0.44 \times 0.44 \times 1 \text{ mm}^3$ . The reconstructions for the other patients were performed accordingly. In a subsequent segmentation step metal artifacts were eliminated and thin bone structures, that got lost due to partial volume effects, were reconstructed.

### 3.2 Alignment of the Pre- and the Postoperative Skull Model

After 3D surface reconstruction, the pre- and the postoperative skull models  $S_1$  and  $S_2$  were registered using an iterative closest point (ICP) algorithm [26]. The alignment was performed for the skull base only, because this region was not affected by the operation (Fig. 7 a). The corresponding regions consisted of approx. 400 000 triangles (200 000 vertices) each. The HAUSDORFF distance  $H = \max(d(S_1, S_2), d(S_2, S_1))$  was minimized, with the postoperative model as a reference [27]. The iterative alignment stopped with a relative deviation of the mean squared distance between two iteration steps below  $10^{-6}$ . The mean value of the two-sided distance  $D$  between the aligned surfaces was in the range of 0.1 and 0.25 mm, depending on the inter-slice distance. Only for approximately 0.5% of the neurocranium, the deviation was above 1 mm, notably at the apex of the skull and the lateral skull base, where the burr holes for the fixation of the external distraction system were located (Fig. 7).

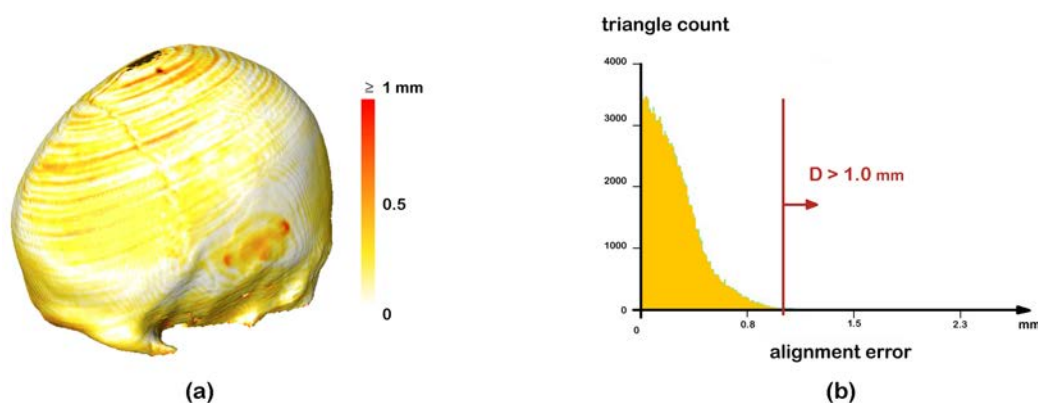


**Fig. 7.** a) color coded alignment error for the neurocranium, b) histogram of the deviation

The transformation, as a result of the ICP alignment, was finally applied to the entire preoperative model, and the deviation between the two models was computed. For the first patient a mean distance of 1.2mm with a standard deviation of 1.5mm and a median of 0.68mm was found, with a maximum deviation for the relocated maxilla of about 15.5mm. Mobile bones like the mandible, the hyoid and the spine exhibited a notable deviation of up to 5mm. An equivalent alignment was performed for all four patient models with similar results.

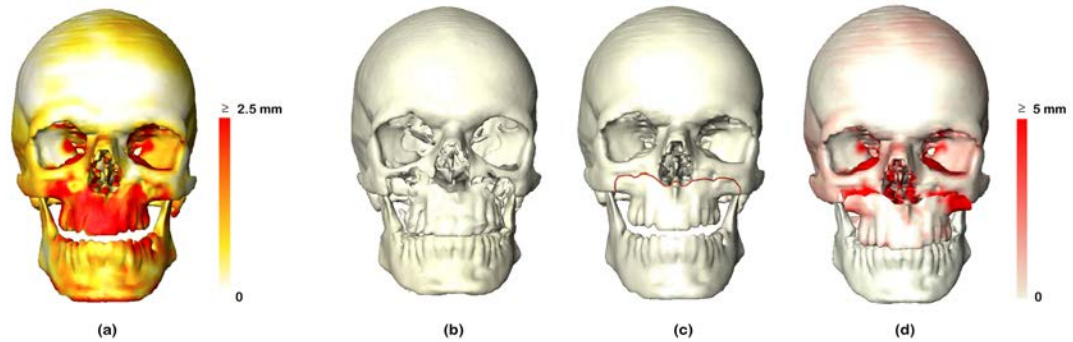


**Fig. 8.** a) color coded deviation on top of the preoperative skull surface, b) postoperative skull reconstruction, c) osteotomy reproduction, d) maxillary advancement and mandible rotation for the preop. model according to the postop. situation with color coded deviation

### 3.3 Osteotomy and Bone Relocation

To compare the soft tissue prediction with the postoperative result, the osteotomy as well as the bone relocation must be reproduced as accurate as possible. Therefore, the distances per triangle were color coded on top of the polygonal surface model (Fig. 8 a), and the osteotomy lines were precisely traced, guided by the deviation of the aligned pre- and postoperative skull model with an appropriately chosen color map (Fig. 8). To reproduce the maxillary advancement, suitable corresponding landmarks were chosen, i.e. prominent points on and between the teeth, as well as the *spina nasalis anterior*, for instance. In a similar manner, anatomical landmarks for the mandible and the spine were specified to compensate for the different positions within the pre- and the postoperative data sets. A landmark based rigid transformation of the maxilla, the mandible, and the spine finally lead to a configuration that accurately mimics the postoperative situation (Fig. 9).

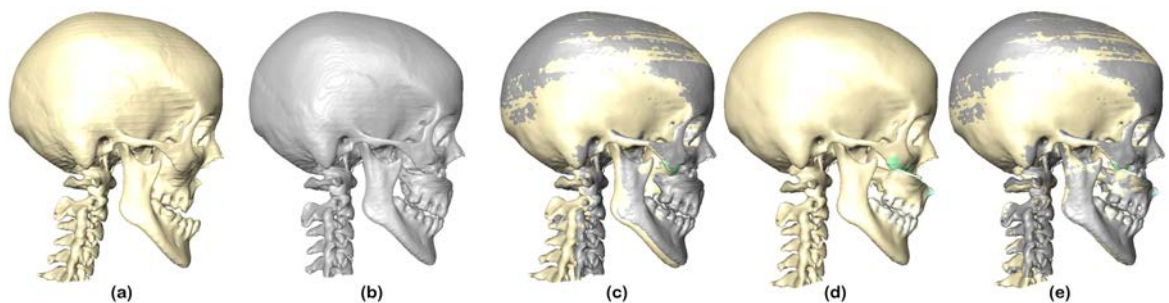


**Fig. 9.** a) Preoperative planning model, b) postoperative model, c) overlay of aligned pre- and postop. models, d) reproduction of the postop. situation and e) overlay with postop. model

### 3.4 Simulation of Soft Tissue Deformation

After surgery planning, the bone displacements are applied to the corresponding boundaries of the tissue grid. Strains are inducing deformation energy that is to be minimized for the determination of an equilibrium state representing the new soft tissue arrangement (see Section 2.3). Using an iterative solver, the computation for a linear elastic model without adaptive refinement takes just a few minutes on a conventional Pentium IV PC with 1 GB RAM. A *qualitative* comparison of the simulated facial appearance with postoperative results is already encouraging (Fig. 10). However, solely a *quantitative* evaluation, being discussed in the remainder of this chapter, will provide reliable information on the prediction quality.

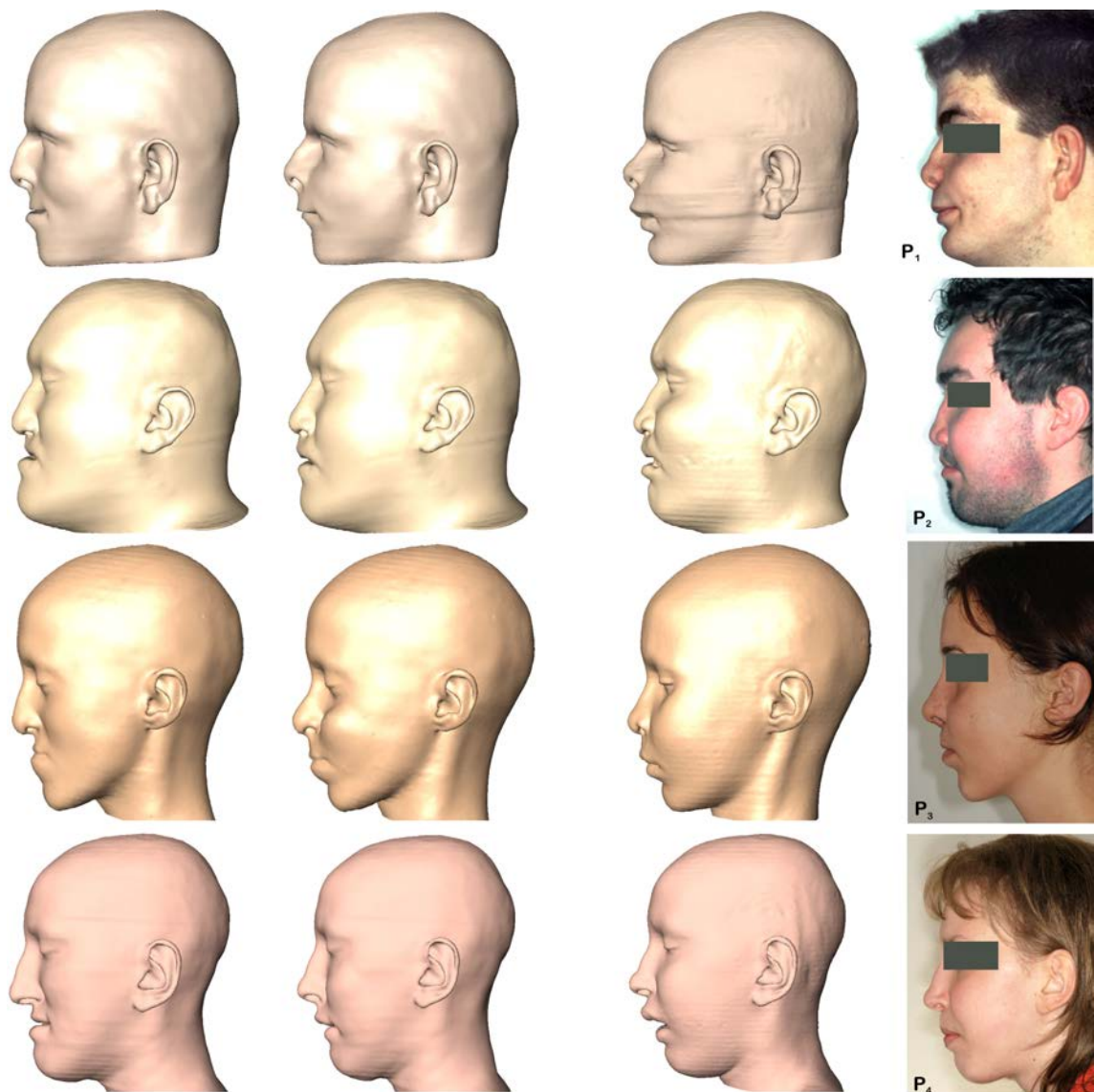


**Fig. 10.** Qualitative comparison of predicted and postoperative results: left) 3D reconstruction from preoperative CT data; middle) prediction after surgery simulation and 3D reconstruction from postoperative CT data, right) postoperative photograph

### 3.5 Quantitative Assessment of the Simulation Results

In a *homogeneous* tissue model, YOUNG's modulus  $E$  has no influence at all on the LAMÉ-NAVIER-equation (3). Therefore, only the value of POISSON's ratio  $\nu$  was varied in a first investigation within the range of  $[0 \dots 0.5]$ . For all of the four patients the two-sided distance between the retrospectively simulated and the postoperative *facial skin surface* was computed, taking into account that 60 % of the head surface is not affected by the maxillary advancement. The mean distance  $D(\nu)$  between the simulated and the postoperative skin surfaces lies between 0.85 mm and 1.15 mm, with a standard deviation of 1.40 mm to 2.64 mm and an *rms* of 1.65 mm to 2.90 mm. In two cases, the best correspondence was found with decreasing values  $\nu \rightarrow 0$  (Fig. 11), that contradicts the common assumption that living tissue is almost incompressible. The inspection of the soft tissue's volume showed that these patients significantly lost weight during the therapy, probably due to reduced chewing capabilities. A tissue model with higher compressibility can partially compensate this difference. However, this has to be further investigated. For the other two patients, a best correspondence was achieved between  $0.43 < \nu < 0.48$ , an observation that coincides with literature values [28, 29].

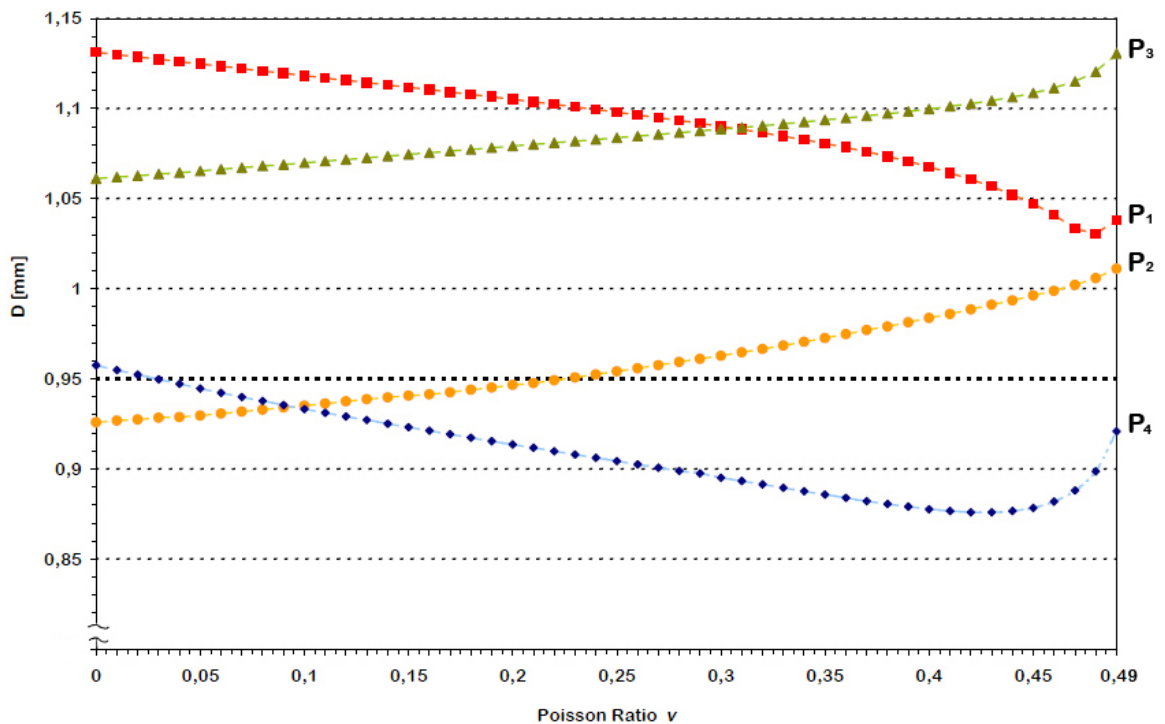


**Fig. 11.** Mean deviation between predicted and postoperative facial skin surface in dependence on POISSON's ratio  $\nu$  for a *homogeneous* soft tissue model

For approximately 70 % of the facial skin surface, the prediction error was below 1 mm, and only 5 to 10 % show a deviation larger than 3 mm. These areas are mainly subjected to postoperative swelling (Fig. 12). However, a mean prediction error of about 1 mm already seems to be an acceptable result for a homogeneous, linear-elastic tissue model.

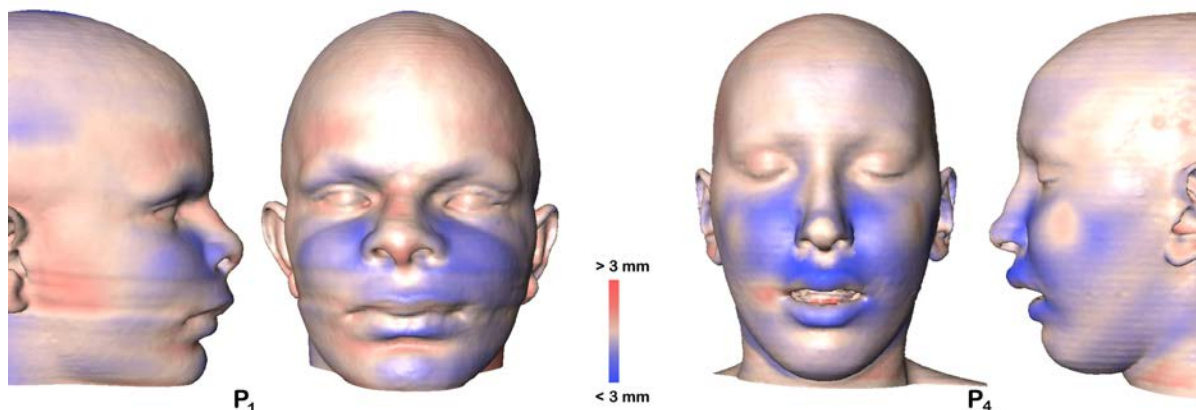


**Fig. 12.** Color coded deviation between prediction and postoperative result for an isotropic, homogeneous linear elastic tissue model

In a second study an *inhomogeneous* tissue model was investigated, where to each tissue element individual histomechanic parameters can be attributed. Unfortunately there is no unique relationship between HOUNSFIELD units and mechanical properties. The determination of appropriate values for different tissue types is still subject of ongoing research in biomechanics and elastography. Thus, literature values that are derived from experiments were taken (Tab. 1).

**Table 1.** Elastic properties of soft tissues, YOUNG's modulus  $E$  ( $1 \text{ Pa} = 1 \text{ N/m}^2$ )

Source	Skin [MPa]	Soft Tissue [kPa]	Fat [kPa]	Muscle [kPa]
Reihnsner, 1989 [30]	4...15	–	–	300
Holzapfel, 2000 [31]	0,1...2...	–	–	–
Elden, 1973 [32]	3,43...157	–	–	–
Azar, 2001 [33]	–	–	4,5...120	–
Duck, 1991 [28]	–	–	–	6,2...300
Maass, 1999 [34]	–	–	20...60	15...264
Krouskop, 1998 [35]	–	6,8...110	20	–
Ophir, 1999 [36]	–	–	20	–
Levinson, 1995 [37]	–	–	–	50...150

In order to preserve the original tissue grid for comparison, we relabeled the tissue elements according to the mean HOUNSFIELD values, using a barycentric sampling with selectable refinement of up to 512 sample points per tetrahedron. At first we differentiated between muscle and embedding tissue, since muscle can easily be segmented within a range of  $[-30, 100]$  HU. As a result, the tissue grid consists of two different tissue types, that can be assigned individual values for  $\nu$  and  $E$ . For each tissue, the POISSON ratio  $\nu$  was varied within the range of  $[0...0.5]$  and YOUNG's modulus  $E$  within  $[50...450]$  kPa. An FE simulation of the tissue deformation has been conducted for each combination to compute  $D(\nu_s, E_s, \nu_m, E_m)$ .

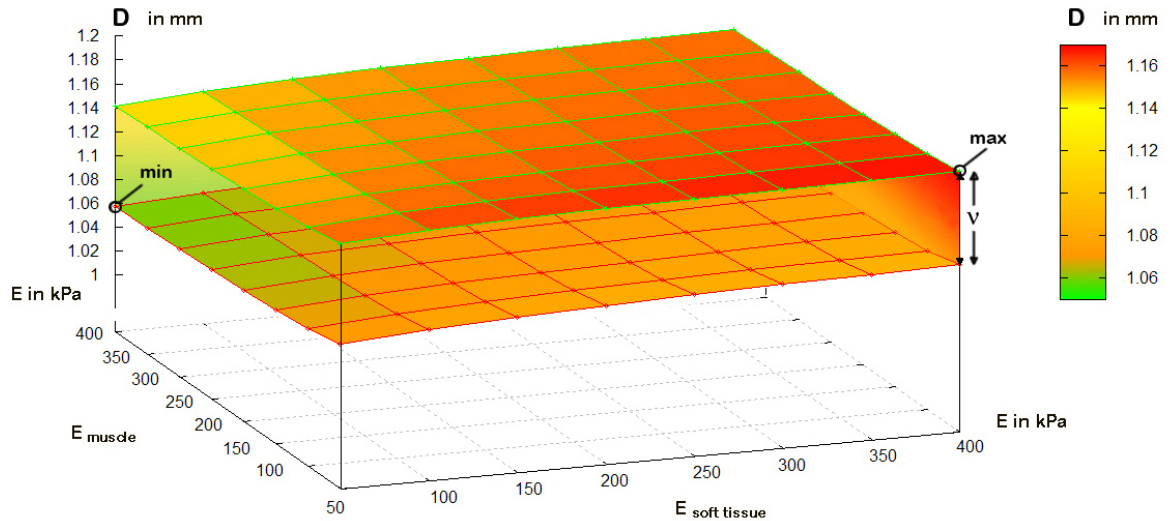


**Fig. 13.** Mean deviation between predicted and postoperative facial skin surface in dependence on YOUNG's moduli  $E$  and POISSON ratios  $\nu$  for an *inhomogeneous* tissue model

All values of  $D$  are located in-between the two colored planes depicted in Figure 13. These two planes are representing the limits of all combinations of  $\nu_s$  and  $\nu_m$  within the given range  $[0 \dots 0.5[$ . Independent of the choice of POISSON's ratio, an optimum was found for YOUNG's modulus  $E_m > 300$  kPa for muscle and  $E_s < 100$  kPa for fatty or connective tissue. In a second run, the tissue deformation has been computed with optimally chosen POISSON ratios, varying the elastic moduli within the range of  $]0, 500]$  kPa at a higher resolution (Fig. 14).

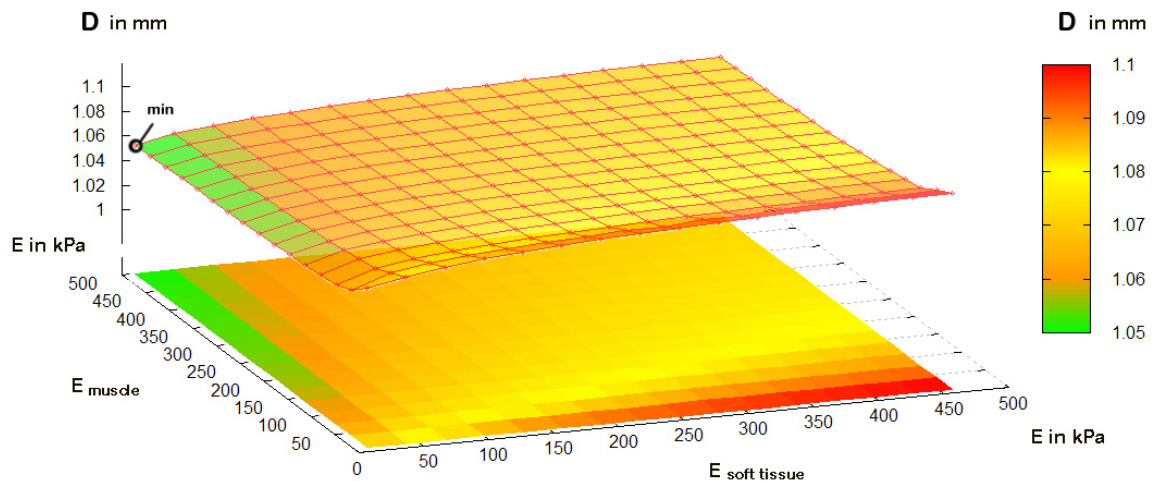


**Fig. 14.** Prediction quality of an *inhomogeneous* tissue model in dependence on YOUNG's moduli  $E$  with optimally chosen POISSON ratios  $\nu$

Although the resulting variation was only small in comparison to the homogeneous tissue model, the inhomogeneous model performed slightly better (cf. Fig. 15 b). The best correspondence was found with  $0.43 < \nu_m < 0.45$  and  $E_m > 300$  kPa for muscle and with  $0.44 < \nu_s < 0.47$  and  $E_s < 50$  kPa for the embedding tissue. However, the net improvement of using inhomogeneous tissue models, or of fine tuning the elastic parameters *does not* significantly influence the prediction quality for the facial skin surface. These values rather have an effect on inner tissue regions of high strains due to large bone displacements, that are typically located at the bone-tissue boundaries. Thus, advanced modeling approaches are to be investigated to improve facial tissue prediction for computer assisted maxillofacial surgery planning.

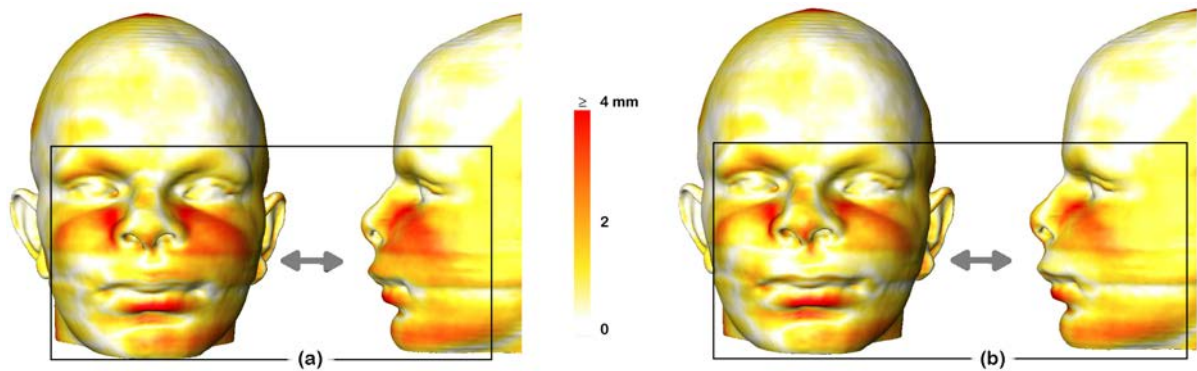


**Fig. 15.** Difference between soft tissue prediction and true postoperative outcome: a) using a homogeneous, and b) an inhomogeneous tissue model

## 4 ADVANCED MODELING APPROACHES

Besides inhomogeneous tissue models, a number of further aspects of more realistic modeling need to be taken into account, some of which are currently under investigation.

### 4.1 Nonlinearity

In the linear-elastic approach (Section 2.3), the CAUCHY strain tensor  $\boldsymbol{\varepsilon}(\mathbf{u}) = \frac{1}{2}(\nabla\mathbf{u} + (\nabla\mathbf{u})^T)$  is a simplification of the GREEN-ST. VENANT strain tensor  $\mathbb{E}(\mathbf{u}) = \frac{1}{2}(\nabla\mathbf{u} + (\nabla\mathbf{u})^T + \nabla\mathbf{u}(\nabla\mathbf{u})^T)$ , which describes the geometry exactly, but depends nonlinearly on  $\mathbf{u}$ . A linearization around the undeformed configuration ( $\mathbf{u} = 0$ ) is only valid for small strains. However, in surgery planning bone relocations of up to 25 mm can thoroughly occur, which cannot be regarded as small displacements anymore. Preliminary results for geometric nonlinearity have been presented in [40, 41], but the proposed method did not address non-convexity and is therefore of limited applicability. Moreover, the linear stress-strain relationship given by the ST. VENANT-KIRCHHOFF constitutive equations is merely a physically correct description of the material response for small strains only. In particular, the solutions of the corresponding LAMÉ-NAVIER equations (3) may exhibit regions of local material interpenetration (i.e. the volume  $\det(I + \nabla\mathbf{u})$  of deformed tissue elements becomes negative).

For a qualitatively correct description of large strains it is necessary that

$$W(\mathbb{E}) \rightarrow \infty \quad \text{for} \quad \det(I + \nabla \mathbf{u}) \rightarrow 0. \quad (5)$$

However, such stored energy functions are necessarily nonconvex, thus complicating the computation of a minimum. An interesting class of constitutive laws are OGDEN materials [42], which include the well-known MOONEY-RIVLIN, neo-HOOKEAN, and VARGA models. For details we refer to [11]. Further hyperelastic material laws that are used in soft tissue modeling are discussed, e.g., in FUNG [29, Chap. 7], HAYASHI [44], and LIU, KERDOK, HOWE [49]. The challenge is to obtain reliable model parameters for living human tissue. First steps towards integrating nonlinear hyperelastic constitutive laws and geometric nonlinearity into our soft tissue prediction have been undertaken [43]. An OGDEN material with stored energy function

$$W(\mathbb{E}) = a \operatorname{tr}(\mathbb{E}) + b \operatorname{tr}(\mathbb{E})^2 + c \operatorname{tr}(\mathbb{E}^2) + d \Gamma(\det(I + \nabla \mathbf{u}))$$

has been used. The parameters  $a, b, c$ , and  $d$  can be adjusted such that a ST. VENANT-KIRCHHOFF material with given YOUNG's modulus  $E$  and POISSON ratio  $\nu$  is approximated to second order accuracy around the undeformed state. Incompressible materials should be considered as well, although the results presented in Section 3.5 indicate that a compressible tissue model might be preferable.

## 4.2 Anisotropy and Inhomogeneity

The consideration of anisotropy also tends to be an issue for tissue modeling. This is particularly the case for muscle and skin, which exhibit a distinct directional behaviour under loading conditions. Therefore, muscle fiber directions and characteristic skin tension lines (so called KRAISSL or LANGER lines) are to be taken into account (Fig. 16).

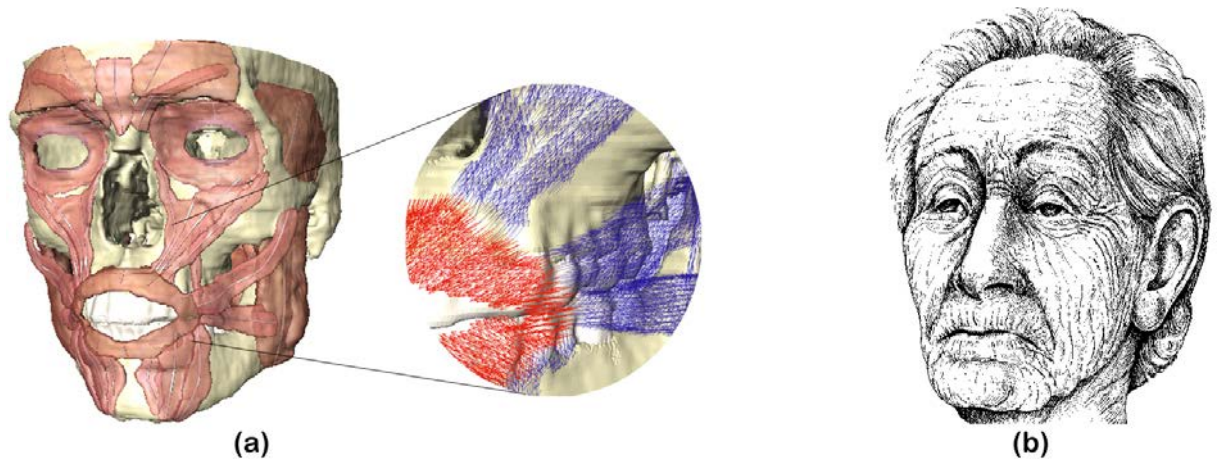


**Fig. 16.** a) muscle fiber directions, derived from anatomy and b) skin tension lines for modeling anisotropy of biological tissues

The tensor of elasticity can thereby be oriented according to a corresponding vector field defined on the nodes of the tetrahedral grid. Such vector fields are easy to construct from geometry or by interactive specification. The usefulness of such an approach, however, is still subject of further investigation. Besides the distinction between muscle and fatty or connective tissue, the separate modeling of a skin layer should improve the prediction quality, due to the different mechanical properties with respect to both, material parameters and orientation of the anisotropy. However, the skin layer is too thin to be efficiently represented by a 3D triangulation. Instead, it seems to be preferable to represent skin by the triangulated surface of the face, to omit bending energy, and to restrict the model to plane stress contributions.

### 4.3 Tissue Remodeling

Up to now, the prediction task has been seen as a static problem of elastomechanics. However, soft tissue exhibits pronounced nonelastic properties on different time scales. For the task of therapy planning, the visco-elastic behavior of biological material on the time scale of seconds to hours can safely be ignored. In contrast, the physiological answer of both soft tissue and bones to the deviation from the homeostatic state caused by the therapy is likely to have a significant impact on the long-term geometry of a patient's face. Taking the effects of tissue remodeling into account, as studied, e.g., by FUNG [29, Chap. 8 and 12], MARTIN et al. [45], and KUHL et al. [46], an improved long-term reliability of facial tissue prediction will be obtained.

### 4.4 Boundary Conditions

The physically correct treatment of the interface between soft tissue and bone remains a challenging task. On large regions of this interface, especially around the osteotomy lines, the soft tissue is not attached firmly to the bone. Tissue is lifted during operation and relocated bone will be covered again afterwards, such that the tissue can slip along the bone surface. Between teeth and oral mucosa, for instance, the contact area where the surrounding tissue rests on the teeth is not known a priori, which leads to a significantly more complex contact problem. This necessitates the application of algorithms from constrained optimization, such as monotone multigrid [47] or interior point methods [48].

### 4.5 Numerical Aspects

Two major goals for designing a useful surgery planning environment are to provide a *fast* and *reliable* computation of volume deformation. In the following we will point out some numerical aspects of soft tissue prediction that have to be addressed in order to meet this requirement.

Since the computing time increases with the tissue grid size, these grids are constructed as coarse as possible without sacrificing relevant geometric details (Section 2.1). For an accurate prediction of the tissue deformation, however, the grid has to be sufficiently fine to also capture all relevant details of the displacement, which is not yet known at the time when the grid is created. Often the grid needs to be refined to represent rapidly varying strains and stresses reliably. In order to keep the grid as coarse as possible, adaptive refinement guided by some local error estimator will be preferred over uniform refinement. Elements are refined iteratively in regions of high approximation error, thus keeping the total number of tetrahedra as low as possible.

In a first step, a hierarchical error estimator [38] has been investigated. In Figure 17, a slight improvement of such a refinement can be seen in the cheek regions where higher strains occur at bony ridges. Since the ultimate goal is a precise prediction of the face, goal oriented error estimator techniques [39] might be advantageous, that emphasize local errors which contribute most to approximation errors of the tissue surface.

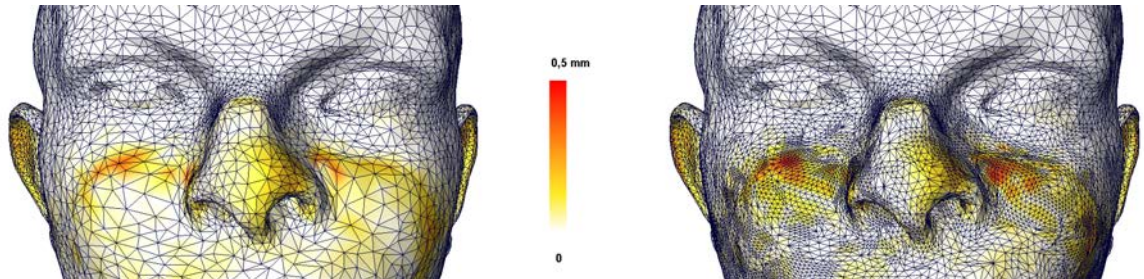


**Fig. 17.** Difference between tissue prediction with and without adaptive mesh refinement

All of the aforementioned refined modeling aspects increase computational complexity and accuracy of the prediction to a different amount. As with the grid size, it will be necessary to study which of them improve the tissue prediction so much as to justify the increase in computation time. When realistic nonlinear hyperelastic material laws are used for simulation, every iterate and in particular the initial guess, needs to locally preserve the material's orientation. A direct application of the displacement of boundary nodes, however, will usually lead to interpenetration. Generating an orientation-preserving initial iterate becomes a nontrivial task. As a remedy, different homotopies may be used to approach the ultimate solution. Possible candidates are a homotopy in the boundary conditions (incremental load), or a homotopy in the nonpenetration barrier shift  $s$ ,  $\det(I + \nabla \mathbf{u}) \geq s$ , from negative values to 0. Both methods have been successfully applied to test examples. A necessary precondition for successful employment of realistic constitutive laws is that the prescribed boundary conditions permit orientation-preserving configurations in the first place. This imposes an additional requirement on the grid generation and necessitates a very careful planning and translation of bone cuts and movement of bony segments into boundary conditions.

## 5 RESULTS AND DISCUSSION

We presented an integrated approach for cranio-maxillofacial surgery planning that comprises the reconstruction of individual 3D patient models from tomographic data, the planning of bone cuts (osteotomies) and relocations of mobilized bone segments, and the numerical simulation of the resulting facial tissue arrangement. The simulation depends on the mathematical modeling approach, the histomechanical model, as well as on the quality of the geometric model. At the moment, the generation of adequate geometric models is the most time consuming task, taking a few hours for segmentation, simplification, and grid generation. We are working on improvements to speed up this process for clinical use. Furthermore, a reliable tissue prediction depends on the correct boundary conditions that immediately result from the relocation

of mobilized bone segments. Such a planning takes approximately 10 to 30 minutes, depending on the complexity of the malformation. The numerical simulation of the resulting tissue deformation does not necessitate any additional user interaction and takes just a few minutes on a conventional PC. It has been shown that 3D soft tissue simulation, based on continuum mechanics, already leads to reasonable results for cranio-maxillofacial surgery planning, even with a homogeneous, linear-elastic tissue model.

The quantitative comparison of the simulation results with the actual postoperative results showed that an inhomogeneous tissue model with embedded muscle regions and properly chosen tissue parameters leads to slightly better results than a homogeneous tissue model. Despite its simplicity, the soft tissue model achieves a mean prediction error of 0.8 to 1.2 mm. From a surgical point of view, this is a quite acceptable result for the assessment of bone relocations with regard to the esthetic outcome, and already enhances the decision process as well as the preoperative patient information tremendously. However, more accurate modeling can be expected to further improve the accuracy and reliability of the predictions.

One noticeable problem for a meaningful validation was the difference between the shapes of the lips (cf. Fig. 10). In the preoperative data sets the upper lips were often located behind the lower ones and both lips were in contact. The postoperative data sets, in contrast, show a more natural shape of the lips due to the surgical correction. For better simulation results, lips and teeth should always be separated during CT data acquisition, e.g. by using a wax plate.

More pre- and postoperative data sets will be compared for validation, and improved modeling approaches will be evaluated. However, postoperative swelling makes it difficult to properly validate the accuracy of soft tissue prediction. Thus, the later postoperative CT data are acquired, the better. In addition to the validation using postoperative CT data, a prospective study is targeted at postoperative investigation of tissue deformation. Skin surface data are to be acquired for a period of 12 months after surgery, either with MRI or with surface digitizers. That way, skin surface development can be recorded and quantified in order to improve the tissue model in view of more reliable prediction of long term results.

Concluding we would like to point out other important sources of prediction errors that from our perspective are prevailing and have to be handled in future modeling approaches. Local adaptive refinement is generally preferred. For very large bone displacements, nonlinear hyperelastic or visco-elastic material models need to be considered. The correct treatment of contact will play a crucial role. Anisotropy, a separate skin layer, and tissue remodeling aspects will also need to be evaluated.

## 6 ACKNOWLEDGEMENTS

We are very grateful to Dr. Dr. Hierl, University Hospital Leipzig, Department of Oral and Maxillofacial Surgery, and Prof. Dr. Klöppel, head of the Radiology Department, for kindly providing us with pre- and postoperative CT data. Furthermore, we would like to acknowledge the cooperation with Prof. Dr. Dr. Zeilhofer, Kantonsspital Basel, and Dr. Westermark, Karolinska Institute in Stockholm, Sweden. Many thanks to all supporting clinicians for their valuable remarks as well as to the patients for their trust in our surgery planning and tissue prediction.

# Bibliography

- [1] Landes CA, Zachar R, Diehl T, and Kovács AF: *Introduction of a three-dimensional anthropometry of the viscerocranium. Part II: Evaluating osseous and soft tissue changes following orthognatic surgery*. J Craniomaxillofac Surg 30, pp. 25–34 (2002)
- [2] Ayache N and Delingette H (eds.): *Surgery Simulation and Soft Tissue Modeling*, Lecture Notes in Computer Science, no. 2673, Springer-Verlag, Tokyo · Berlin · Heidelberg (2003)
- [3] Cotin S and Metaxas D (eds.): *Medical Simulation*, Lecture Notes in Computer Science, no. 3078, Springer-Verlag, Tokyo · Berlin · Heidelberg (2004)
- [4] Zachow S, Gladilin E, Hege HC, and Deuffhard P: *Finite-element simulation of soft tissue deformation*. In: Proc. CARS 2000, pp. 23–28 (2000)
- [5] Stalling D, Westerhoff M, Hege, HC, et al.: *Amira: A Highly Interactive System for Visual Data Analysis*, in: Hansen CD and Johnson CR (eds.), The Visualization Handbook, chapter 38, pp. 749–767 (2005) URL: [amira.zib.de](http://amira.zib.de)
- [6] Koch RM: *Methods for physics based facial surgery prediction*. Dissertation No. 13912, ETH Zürich (2000)
- [7] Teschner M: *Direct computation of soft-tissue deformation in craniofacial surgery simulation*. Dissertation, Friedrich-Alexander-Universität Erlangen-Nürnberg (2000)
- [8] Barré S: *Modélisation, fusion et reconstruction 3D pour l'aide à la chirurgie maxillo-faciale*. Dissertation, Université de Poitiers (2001)
- [9] Chabanas M.: *Modélisation des tissus mous de la face pour la chirurgie assistée par ordinateur*. Dissertation, Université Joseph-Fourier - Grenoble (2004)
- [10] Zachow S, Gladilin E, Sader R, and Zeilhofer HF: *Improved 3D Osteotomy Planning in Cranio-Maxillofacial Surgery*. In: Springer Lecture Notes in Computer Science, Proc. Medical Image Computing and Computer-Assisted Intervention, pp. 473–481 (2001)
- [11] Ciarlet PG: *Mathematical Elasticity: Three-Dimensional Elasticity*, vol. 20 of Studies in Mathematics and its Applications, North-Holland, Amsterdam (1988)
- [12] Hege HC, Seebaß M, Stalling D, and Zöckler M.: *A generalized marching cubes algorithm based on non-binary classifications*. Zuse-Institute Berlin ZIB Preprint SC-97-05 (1997)
- [13] Stalling D, Zöckler M, and Hege HC: *Interactive Segmentation of 3D Medical Images with Subvoxel Accuracy*. In: Proc. CAR'98, pp. 137–142 (1998)
- [14] Garland M and Heckbert PS: *Simplification using quadric error metrics*. In: Proc. of SigGraph, ACM Computer Graphics 1997, pp. 209–216 (1997)
- [15] Lo SH: *Automatic mesh generation over intersecting surfaces*. Int. Journal for Numerical Methods in Engineering 44, pp. 1359–1376 (1995)
- [16] Rassineux A: *Generation and optimization of tetrahedral meshes by advancing front technique*. Int. Journal for Numerical Methods in Engineering 41, pp 651–674 (1998)
- [17] Zachow S, Gladilin E, Sader R, and Zeilhofer HF: *Draw & Cut: Intuitive 3D Osteotomy planning on polygonal bone models*. In: Proc. CARS 2003, pp. 362–369 (2003)
- [18] Buzug Th and Lüth T: *Perspectives in Image-Guided Surgery*. Proc. VDE Scientific Workshop on Medical Robotics, Navigation and Visualization MRNV (2004)
- [19] Braess D: *Theory, Fast Solvers, and Applications in Solid Mechanics*. Cambridge University Press, 2nd edition (2001), ISBN 0521011957
- [20] Erdmann B, Beck R, Deuffhard P, et al.: *Kaskade - An Adaptive Multilevel Finite-Element Software*, URL: [www.zib.de/Numerik/numsoft/kaskade](http://www.zib.de/Numerik/numsoft/kaskade)
- [21] Kerdok AE, Cotin SM, Ottensmeyer MP, Galea AM et al.: *Truth cube: Establishing physical standards for real time soft tissue simulation*. Medical Image Analysis 7, pp. 283–291 (2003)
- [22] Hierl T and Hemprich A: *A novel modular retention system for midfacial distraction osteogenesis*. Br. J. Oral Maxillofac Surg 38, pp. 623–626 (2000)
- [23] Hierl T, Klisch M, Klöppel R, and Hemprich A: *Therapie ausgeprägter Mittelgesichtsrücklagen mit Hilfe der Distractionosteogenese*. Mund-, Kiefer- und Gesichtschirurgie 7(1), pp. 7–13 (2003)
- [24] Klöppel R, Hierl Th, Gosch D, et al.: *Kallusdistraction des Mittelgesichts: Anforderungen an die bildgebende Diagnostik*. Radiologie 39, pp. 1068–1078 (1999)
- [25] Zachow S, Hierl Th and Erdmann B: *On the predictability of tissue changes for osteotomy planning in maxillofacial surgery: A comparison with postoperative results*. In: Proc. CARS 2004, pp. 648–653 (2004)
- [26] Besl PJ and McKay ND: *A method for registration of 3D shapes*. IEEE Trans. on Pattern Analysis and Machine Intelligence 14(2), pp. 239–256 (1992)
- [27] Aspert N, Santa-Cruz D, and Ebrahimi T: *MESH: Measuring errors between surfaces using the HAUSDORFF distance*. In: Proc. IEEE ICME, vol. 1, pp. 705–708 (2002)

- [28] Duck FA: *Physical Properties of Tissue – A Comprehensive Reference Book*. Academic Press, chap. 5, pp. 137 ff. (1991)
- [29] Fung YC: *Biomechanics: Mechanical Properties of Living Tissues*. 2nd edition, Springer (1993)
- [30] Reihnsner R: *Biomechanische Eigenschaften des kollagenen Bindegewebes*. In: *Das kollagene Bindegewebe: Symposium*, Mallinger R and Neumüller J (eds.), Wien (1988), pp. 30–41
- [31] Holzapfel GH: *Biomechanics of soft tissue*. In: *Handbook of Material Behaviour: Nonlinear Models and Properties*, Lemaitre J and Cachan LMT (eds.), Academic Press Inc., No. 7 in Biomech Reprint Series, pp. 1–12 (2000)
- [32] Elden HR (ed.): *Biophysical Properties of the Skin*. Interscience, John Wiley and Sons, Inc., New York (1973)
- [33] Azar FS, Metaxas DN, and Schnall MD: *A deformable finite element model of the breast for predicting mechanical deformations under external perturbations*. In: Proc. of the Int. workshop on deformable modeling and soft tissue simulation (2001)
- [34] Maaß H: *Untersuchung einer Methode zur nichtinvasiven Messung von Steifigkeitskoeffizienten an lebendem Gewebe mit multimodalen bildgebenden Verfahren*. Dissert. Fak. Maschinenbau, Universität Fridericiana zu Karlsruhe (1999)
- [35] Krouskop TA, Wheeler TM, Kallel F, Garra BS, et al.: *Elastic moduli of breast and prostate tissues under compression*. *Ultrasonic Imaging* 20, pp. 260–274 (1998)
- [36] Ophir J, Alam SK, Garra B, Kallel F, et al.: *Elastography: Ultrasonic estimation and imaging of the elastic properties of tissues*. *Journal of Eng. in Medicine* 213(3), pp. 203–233 (1999)
- [37] Levinson SF, Shinagawa M, and Sato T: *Sonoelastic determination of human skeletal muscle elasticity*. *Journal for Biomechanics* 28(10), pp. 1145–1154 (1995)
- [38] Deuffhard P, Leinen P and Yserentant H: *Concepts of an adaptive hierarchical finite element code*. *IMPACT Comp. Sci. Eng.* 1, pp. 3–35 (1989)
- [39] Rannacher R, Suttmeier F-T: *A feed-back approach to error control in finite element methods: Application to linear elasticity*. *Comput. Mech.* 19(5), pp. 434–446 (1997)
- [40] Gladilin E, Zachow S, Deuffhard P, and Hege HC: *Adaptive nonlinear elastic FEM for realistic prediction of soft tissue in craniofacial surgery simulations*. In: Proc. SPIE Medical Imaging 2002: Visualization, Image-Guided Procedures, and Display, pp. 1–8 (2002)
- [41] Gladilin E, Zachow S, Deuffhard P, and Hege HC: *A Comparison of Physical Models of Deformable Soft Tissue for Craniofacial Surgery*. In: Proc. CARS 2003, pp. 343–348 (2003)
- [42] Ogden RW: *Non-Linear Elastic Deformations*, Ellis Horwood, Chichester, and John Wiley (1984)
- [43] Weiser M, Deuffhard P and Erdmann B: *Affine conjugate adaptive Newton methods for nonlinear elastomechanics*. ZIB-Report 04-01 (2004)
- [44] Hayashi K: *Mechanical Properties of Soft Tissues and Arterial Walls*. In Holzapfel GA and Ogden RW (eds.): *Biomechanics of Soft Tissue in Cardiovascular Systems*. Springer (2003)
- [45] Martin RB, Burr DB, and Sharkey NA: *Skeletal Tissue Mechanics*. Springer (1998)
- [46] Kuhl E, Garikipati K, Arruda E, and Grosh K: *Remodeling of biological tissue: Mechanically induced reorientation of a transversely isotropic chain network*. Preprint (2004)
- [47] Kornhuber R: *Adaptive Monotone Multigrid Methods for Nonlinear Variational Problems*. Teubner (1997)
- [48] Wright SJ: *Primal-dual interior-point methods*. Philadelphia, SIAM (1997)
- [49] Liu Y, Kerdok AE, and Howe RD: *A nonlinear finite element model of soft tissue indentation*. In: [3], pp. 67–76 (2004)